

## Mapping out the Stellar Populations of IC 2602 and IC 2391

AZMAIN H. NISAK,<sup>1</sup> RUSSEL J. WHITE,<sup>1</sup> ALEXANDRA YEP,<sup>1</sup> TODD J. HENRY,<sup>1</sup> LEONARDO PAREDES,<sup>1</sup>  
HODARI-SADIKI JAMES,<sup>1</sup> AND WEI-CHUN JAO<sup>1</sup>

<sup>1</sup>*Astronomy Department, Georgia State University, Atlanta, GA 30303*

(Received December 1, 2021)

Submitted to ApJ

### ABSTRACT

IC 2391 and IC 2602 are important benchmarks for testing early star and planet evolution theories, both structural and dynamical, because they are the nearest open clusters with ages of  $\sim 50$  Myr. We refine membership lists for these clusters by identifying candidate members using *Gaia* DR2 kinematic and distance information. We identify 451 candidate members of IC 2602 and 350 candidate members of IC 2391. If confirmed, this would increase the known populations of these clusters by 275% and 130% respectively. We use CHIRON on the CTIO/SMARTS 1.5-m telescope via fiber mode which yields a resolution of 27,400 to acquire high resolution spectra of 26 new candidate cluster members brighter than  $G=13$  magnitude, as well as an additional 12 previously known members. Measures of lithium,  $H\alpha$ , stellar properties (Teff,  $\log(g)$ ,  $[Fe/H]$ ), radial velocities, and  $v \sin i$  values from these spectra are used to confirm cluster membership. We find that 37 of 38 stars we observe are bona-fide cluster members, of which 4 are new candidate photometric binaries and 10 are new candidate spectroscopic binaries.

**Keywords:** Hertzsprung-Russell and C-M diagrams — open clusters and associations: general — open clusters and associations: individual (IC 2602, IC 2391) — stars: fundamental parameters — stars: kinematics and dynamics)

### 1. INTRODUCTION

IC 2602 and IC 2391 are nearby ( $\sim 150$  pc; Bravi et al. 2018) open clusters located in the Carina and Vela constellations respectively. Despite being spatially close on the sky (within 30 degrees), the clusters differ in their space motions and likely do not share a common origin; the mean radial velocities of IC 2602 and IC 2391 are estimated to be  $17.4 \pm 1.0$  km/s (Marsden et al. 2009) and  $14.8 \pm 0.7$  km/s (Platais et al. 2007) respectively. It is believed that IC 2602 formed in conjunction with the Local association, otherwise known as the Pleiades supercluster (Eggen 1975, 1983a,b), while IC 2391 formed alongside the Argus association (Torres et al. 2008, De Silva et al. 2013) as part of the IC 2391 supercluster

(Eggen 1991). IC 2602 and IC 2391 experience low reddening with estimated  $E(B-V)$  values of  $0.068 \pm 0.025$  and  $0.088 \pm 0.027$  respectively.

Spectra of their main-sequence FGK stars reveal that IC 2602 and IC 2391 have near-solar metallicities of  $0.00 \pm 0.01$  and  $0.06 \pm 0.06$  respectively (Randich et al. 2001, 2002; Platais et al. 2007; D’Orazi & Randich 2009; Marsden et al. 2009; Boudreault & Bailer-Jones 2009; Spina et al. 2017). Age estimates for IC 2602 and IC 2391 are determined to be  $43.7^{+4.3}_{-3.9}$  and  $51.3^{+5.0}_{-4.5}$  Myr respectively, which are inferred by modeling the lithium depletion boundary and chasm (Barrado y Navascués et al. 2004; Dobbie et al. 2010; Bravi et al. 2018). The age estimates are consistent with those determined from the main sequence turnoff ( $\sim 30$ -50 Myr), which is potentially plagued by rapid rotation and gravity darkening (Jones et al. 2015; Brandt & Huang 2015; Cummings et al. 2017; Randich et al. 2018).

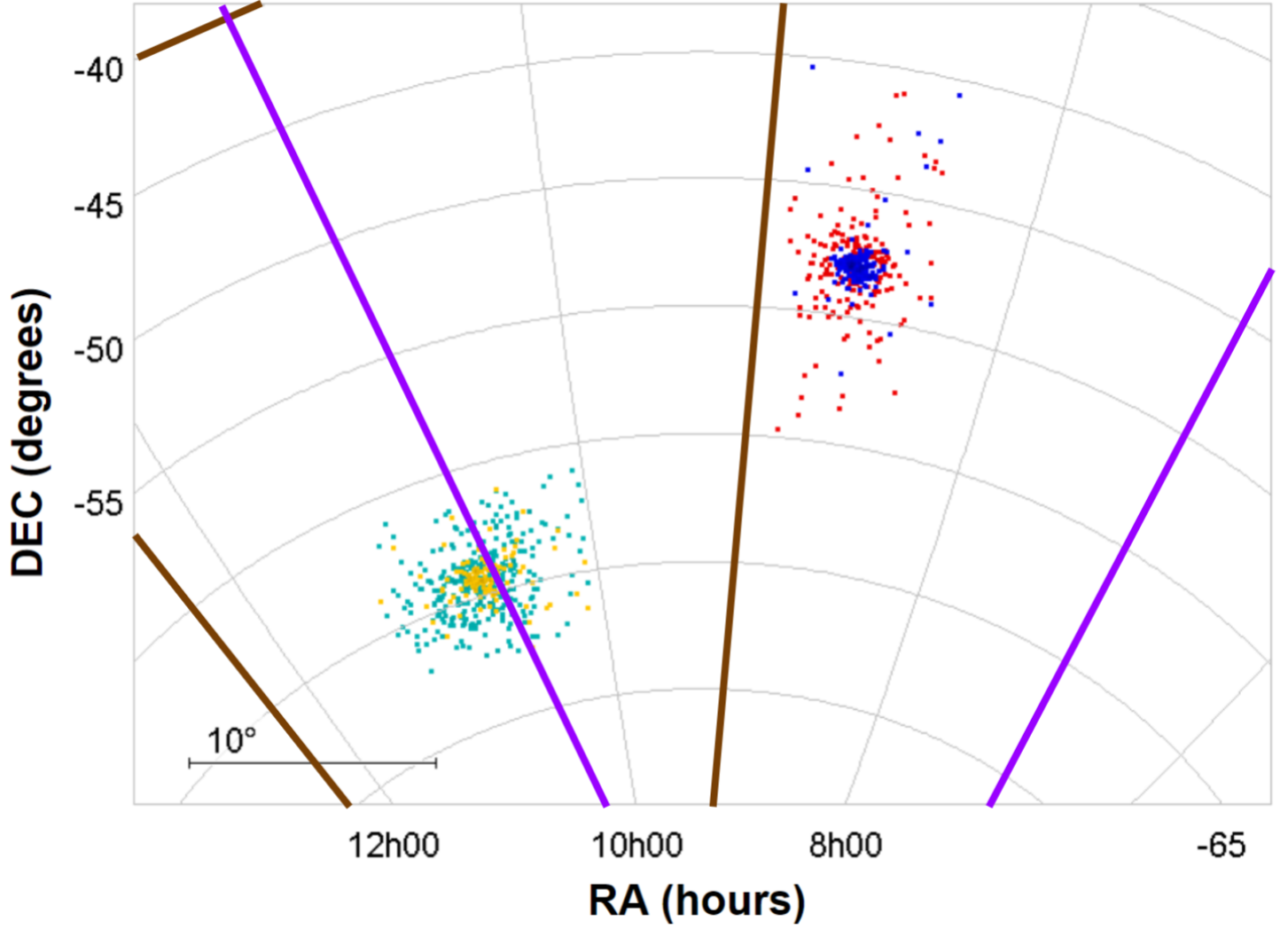


**Figure 1.** Sky positions for IC 2602 and IC 2391 candidate cluster members identified using the prescription in Section 2. The RA and DEC ranges of search regions are shown and extend off the plot (brown for IC 2602 and purple for IC 2391). New and known IC 2391 candidate members are represented by red and blue points, respectively. New and known IC 2602 candidate members are represented by cyan and yellow points, respectively.

Given their close proximity and age, IC 2602 and IC 2391 are important benchmark clusters because they are the closest clusters with ages intermediate between that of star forming regions ( $< 10$  Myr) and that of well-studied open clusters ( $> 100$  Myr; Lada & Lada 2003). At these transitional ages, low mass stars are still gravitationally settling towards the main sequence (Baraffe et al. 2015) and planetary systems are in the process of dynamically evolving (Quinn & White 2016; Mann et al. 2017; Gaidos et al. 2017; Ragusa et al. 2018).

To study these clusters in detail, a plethora of investigations have been undertaken to identify potential candidate members of IC 2602 and IC 2391 via parallax, proper motion, spatial extent, and photometry (Whiteoak 1961; Feinstein 1961; Braes 1962; Lyngå 1962; Foster et al. 1997; Rolleston & Byrne 1997; Simon & Patten 1998; Barrado y Navascués et al. 2001; Dodd 2004; Randich et al. 2005; Gagné et al. 2018). Additionally, numerous spectroscopic studies have been conducted to confirm candidate members via signatures of youth (e.g. lithium,  $H\alpha$ , large  $v \sin i$ ) and stellar properties consistent with those of bona-fide cluster members (Buscombe 1965; Abt & Morgan 1972; Levato et al. 1988; Messina et al. 2003; Paulson & Yelda 2006; Platais et al. 2007; Mermilliod et al. 2009; De Silva et al. 2013; Merle et al. 2017; D’Orazi et al. 2017). Both clusters appear to harbor a population of brown dwarfs (Barrado y Navascués et al. 2004; Dobbie et al. 2010).

The European Space Agency’s *Gaia* satellite has revolutionized our capacity to recognize and characterize Galactic star clusters and has the potential to significantly refine membership lists for open clusters (Cantat-Gaudin et al. 2018; Lodiou et al. 2019; Zuckerman et al. 2019). However, while the *Gaia* Collaboration’s prescription is largely successful in identifying candidate cluster members (Gaia Collaboration et al. 2018), the prescription is still known to miss bona-fide members in some instances (Zuckerman et al. 2019). Furthermore, stars retrieved from *Gaia* are still only candidate members until confirmed with spectra because even the best samples are affected by contamination from field stars (Briceno et al. 2018).

In the current work, we utilize the second data release (*Gaia* DR2; Gaia Collaboration et al. 2018), which provides kinematic and distance information for over 1 billion stars, to identify potential candidate members of IC 2602 and IC 2391 (Section 2). We obtain high-dispersion optical spectra for all newly identified candidate members of IC 2602 and IC 2391 brighter than  $G=13$  magnitude (Section 3). We use the spectra to measure youth diagnostics, radial and projected rotational velocities, as well as determine stellar properties for each star (Section

**Table 1.** Properties of Candidate Cluster Members

Cluster	Property	Constraint
IC 2602	RA (hr)	$10 \leq \text{RA} \leq 11.3$
	DEC (deg)	$-67.5 \leq \text{DEC} \leq -61$
	$\varpi$ (mas)	$6.2 \leq \varpi \leq 7.0$
	$\mu_\alpha \cos \delta$ (mas/yr)	$-25 \leq \mu_\alpha \cos \delta \leq -10$
	$\mu_\delta$ (mas/yr)	$6 \leq \mu_\delta \leq 17$
	$\epsilon_\varpi$ (mas)	$\epsilon_\varpi \leq 0.5$ (if $G \leq 8$ ) $\epsilon_\varpi \leq 0.35$ (if $G > 8$ )
	$\epsilon_{\mu_\alpha \cos \delta}$ (mas/yr)	$\epsilon_{\mu_\alpha \cos \delta} \leq 0.8$
	$\epsilon_{\mu_\delta}$ (mas/yr)	$\epsilon_{\mu_\delta} \leq 0.8$
IC 2391	RA (hr)	$8.3 \leq \text{RA} \leq 9$
	DEC (deg)	$-60 \leq \text{DEC} \leq -45$
	$\varpi$ (mas)	$6.2 \leq \varpi \leq 7.4$
	$\mu_\alpha \cos \delta$ (mas/yr)	$-31 \leq \mu_\alpha \cos \delta \leq -19$
	$\mu_\delta$ (mas/yr)	$15 \leq \mu_\delta \leq 28$
	$\epsilon_\varpi$ (mas)	$\epsilon_\varpi \leq 0.5$ (if $G \leq 8$ ) $\epsilon_\varpi \leq 0.35$ (if $G > 8$ )
	$\epsilon_{\mu_\alpha \cos \delta}$ (mas/yr)	$\epsilon_{\mu_\alpha \cos \delta} \leq 0.8$
	$\epsilon_{\mu_\delta}$ (mas/yr)	$\epsilon_{\mu_\delta} \leq 0.8$

*Notes.* Candidate cluster members are identified based on right-ascension (RA), declination (DEC), parallax ( $\varpi$ ), proper motion in right ascension ( $\mu_\alpha \cos \delta$ ), and proper motion in declination ( $\mu_\delta$ ), as well as uncertainties of parallax ( $\epsilon_\varpi$ ) and proper motion ( $\epsilon_{\mu_\alpha \cos \delta}, \epsilon_{\mu_\delta}$ ).

3). These measurements allow us to identify new candidate binaries (Section 4), assess cluster membership (Section 5), and characterize ensemble cluster properties (Section 6).

## 2. USING *Gaia* DR2 TO IDENTIFY CANDIDATE CLUSTER MEMBERS

We query the *Gaia* DR2 archive for candidate cluster members with declination and right ascension boundaries centered about the average SIMBAD coordinates (Wu et al. 2009) of bona-fide members ( $160^\circ$ ,  $-65^\circ$  for IC 2602;  $130^\circ$ ,  $-53^\circ$  for IC 2391). The boundaries extend  $25^\circ$  in DEC and 1.7 hr in RA (Figure 1). Within these regions, we identify candidate cluster members using the constraints listed in Table 1 on parallax, proper motion, and measurement uncertainties. We apply a less strict parallax uncertainty constraint for stars brighter than  $G = 8$  mag (0.5 vs. 0.35 mas), based on the recommendations of Drimmel et al. (2019); brighter stars have parallaxes with larger systematic errors.

This prescription identifies 451 candidate members of IC 2602, with  $G$  magnitudes spanning from 4.7 to 19.5. Likewise, it identifies 350 candidate members of IC 2391 with  $G$  magnitudes spanning from 3.5 to 19.6. These stars are plotted on color-magnitude diagrams in Figure 2.

Considering candidate members with  $G < 14$ , our membership lists agree with those of the *Gaia* collaboration (Gaia Collaboration et al. 2018) to 90% (96 stars) and 95% (78 stars) for IC 2602 and IC 2391, respectively. Over the full magnitude range, our prescription yields 46 and 54 candidate members of IC 2602 and IC 2391, respectively, that are not present in the *Gaia* Collaboration’s membership lists. For  $G < 14$ , we identify 13 and 4 candidate members of IC 2602 and IC 2391, respectively, are identified by the *Gaia* Collaboration, but not by the prescription used in this work. While the single-star main sequences are well-defined for these populations overall, they broaden for  $G > 15$  due to larger distance errors; median parallax uncertainties for both clusters are 0.03 mas ( $G < 15$ ), 0.07 mas ( $15 < G < 17$ ), and 0.12 mas ( $17 < G$ ; Gaia Collaboration et al. 2018).

To determine which of our candidate members are known members of these clusters independent of those proposed by the *Gaia* Collaboration, we conduct a cross-match with SIMBAD (Wenger et al. 2000) through Vizier’s X-Match (Ochsenbein et al. 2000) within a 1 arc-second radius of the *Gaia* DR2 coordinates. A candidate member is considered to be a known member if (1) the star is present in SIMBAD and (2) the star has been previously classified as a candidate member of the cluster. From this, we determine that our membership lists contain 120 known members and 331 new candidate members for IC 2602, and 152 known members and 198 new candidate members for IC 2391 (see Figure 2 and 3). If these new candidate members are confirmed, the known stellar populations of these clusters will increase by 275% and 130% respectively.

Renormalized unit weight error (RUWE) values are used in some papers to assess membership of candidate cluster members (Lindgren et al. 2018; Esplin & Luhman 2019; Luhman & Esplin 2020). We don’t use RUWE constraints because bright stars and photometric binaries are preferentially excluded. Bright stars are lost because they have large systematic errors in *Gaia* DR2 astrometry (Drimmel et al. 2019) while photometric binaries are lost because the astrometric  $\chi^2$  relies on a single-star model.

Our new refined membership lists can be found in Appendix tables A.1 (for IC 2391) and A.2 (for IC 2602). The lists are sorted by *Gaia* BP-RP color. For some stars (4 in IC 2391 and 10 in IC 2602), BP-RP color was

not provided. Furthermore, the 3 stars with BP-RP  $< 1$  and  $G > 13$  are unlikely to be white dwarfs based on their ages. If the *Gaia* photometry is correct for these, follow-up spectroscopy may confirm them to be background giants (Richer et al. 2021). Because these stars still show similar distance and space motion as per our prescription, we consider them to be candidate members.

### 3. SPECTROSCOPIC OBSERVATIONS AND PROPERTIES OF CANDIDATE CLUSTER MEMBERS

To confirm the membership candidates identified here, we initiate a spectroscopic survey project to acquire high resolution spectra. We obtain spectra for all 26 bright ( $G < 13$ ) candidate members newly identified in this study to confirm cluster membership. We also observe 12 previously known (also with  $G < 13$ ) cluster members to check the reliability of our analysis techniques. We obtain single-epoch 1200s exposures for each star using the CHIRON echelle spectrograph (Tokovinin et al. 2013; L. Paredes et al. 2021, in preparation) on the CTIO/SMARTS 1.5-m telescope. The stars are observed in fiber mode, which covers 4500-8900 Å over 62 spectral orders at a resolving power of  $R \sim 27,400$ . We also obtain a thorium-argon lamp spectrum before each object spectrum for wavelength calibration. The RECONS team at Georgia State University process the observed echelle spectra from CHIRON to provide wavelength-calibrated spectral orders, as described in Tokovinin et al. (2013). In order to measure radial and projected rotational velocities, single-epoch spectra of CHIRON standards<sup>1</sup> (A. Yep et al. in preparation) are also obtained using the same spectral setup.

#### 3.1. $Li\ I\ \lambda 6708\ \text{\AA}$ & $H\alpha$ Equivalent Widths

As a first assessment of stellar youth, we measure equivalent widths of the lithium doublet at 6708 Å and the  $H\alpha$  feature at 6563 Å using IRAF’s Gaussian-fitting *splot* package. We estimate equivalent width uncertainties using the spectrograph pixel-wavelength scale  $p$  (0.097 Å at  $H\alpha$ ; 0.100 Å at lithium), the measured Gaussian full-width at half maximum  $f$  of the spectral line, and the signal-to-noise ratio (SNR) per pixel, following the prescription of Cayrel (1988) and Deliyannis et al. 1993, 2019):

$$\Delta EW \simeq 1.5 \frac{\sqrt{fp}}{SNR} \quad (1)$$

<sup>1</sup> [https://github.com/alexandrayep/CHIRON\\_Standards](https://github.com/alexandrayep/CHIRON_Standards)

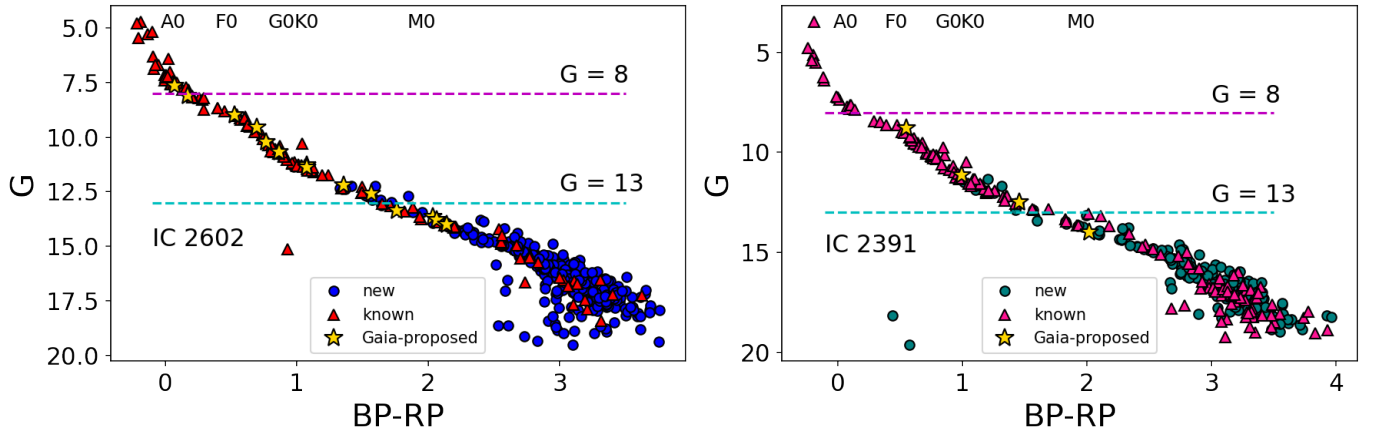


**Figure 2.** *Gaia* apparent  $G$  magnitude versus *Gaia* BP-RP color for 451 candidate members of IC 2602 (*left panel*) and 350 candidate members of IC 2391 (*right panel*); the 14 candidate members without *Gaia* colors (4 in IC 2391 and 10 in IC 2602) are not plotted. For IC 2602, 331 are new (blue circles) while 120 are known (red triangles). For IC 2391, 198 are new (teal circles) while 152 are known (pink triangles). Objects brighter than  $G=14$  in the *Gaia* DR2 membership lists that are absent from ours are indicated by golden stars. The magenta line shows the brightness ( $G=8$ ) above which a more lenient parallax constraint is applied in identifying membership (see Section 2). Estimated spectral types are shown at their corresponding *Gaia* color (Pecaut & Mamajek 2013). We obtain optical spectra for all new candidate members brighter than  $G=13$  (see Section 3).



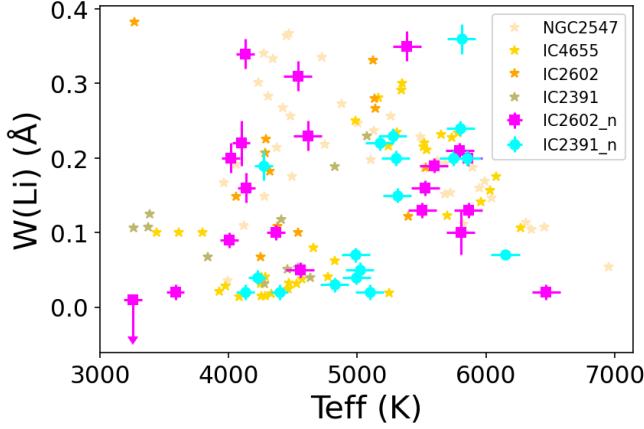


**Figure 3.** Equivalent widths of lithium at 6708 Å are plotted against effective temperatures (see Section 3.3) for all observed stars in this study for IC 2602 (magenta squares; IC2602\_n) and IC 2391 (cyan circles; IC2391\_n). Upper limits are indicated with arrows. Here, we show that our lithium measurements for IC 2602 and IC 2391 are consistent with those for other clusters of similar age (Gutiérrez Albarrán et al. 2020).

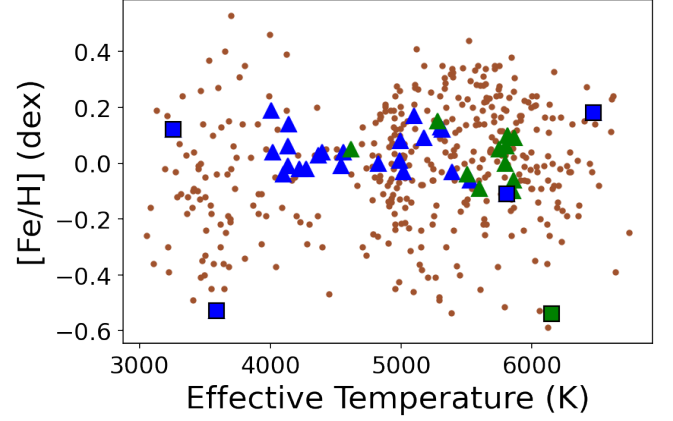


**Figure 4.** Metallicity is plotted against effective temperature for the 393 spectral standards (dwarf stars with  $3 < \log(g) < 5$ ) used in the Empirical SpecMatch spectral library (red points). Previously known members and new candidate members observed in this study are colored green and blue, respectively. Stars are marked as squares if they are candidate double-lined spectroscopic binaries (see Section 4.2) and triangles if they are not.

When reporting equivalent widths, we adopt the standard convention of assigning negative values for emission lines and positive values for absorption. Upper limits are assigned when the spectral line cannot be distinguished from the noise of the continuum. For the candidate double-lined spectroscopic binaries (see Section 4.2), equivalent widths are diminished due to the companion's continuum. The measured equivalent widths of lithium absorption are plotted as a function of effective temperature in Figure 3. The distributions of values are consistent with measurements in clusters with similar age (30-50 Myr based on their main-sequence turnoffs) from Gutiérrez Albarrán et al. (2020). Compared with literature values in previously known members (as reported by Randich et al. 1997, 2001; Platais et al. 2007), our measured values agree within measurement uncertainties ( $\sim 0.02$  Å). Equivalent width values are listed in Tables 3 and 4. New candidate members are designated with the internal identifiers ALN if they are in IC 2602 and NTC if they are in IC 2391.

### 3.2. Radial & Rotational Velocities

To measure the radial velocities (RV) and projected rotational velocities ( $v \sin i$ ) of target stars, we perform normalized cross-correlation of 12 spectral orders (4990-6860 Å). We avoid those with telluric absorption (e.g. A-band, B-band), chromospheric emission (e.g. H $\alpha$ ), and pressure-sensitive lines that may bias the  $v \sin i$  results, between the target and three spectral standards of similar *Gaia* BP-RP color.

A radial velocity is determined from each spectral order by fitting the peak of the cross-correlation function (CCF) with a Gaussian. The radial velocity uncertainty for each spectral order is estimated using the equation from Butler et al. (1996). By weighing these relative radial velocities by their corresponding Doppler uncertainties, a weighted mean relative radial velocity is calculated. Barycentric velocities are determined using EXOFAST's (Eastman et al. 2013) barycentric correction algorithm (Wright & Eastman 2014) and PyAstronomy's *helcorr* function.

We determine projected rotational velocities by creating an empirical relation between the CCF width and  $v \sin i$ , by cross-correlating each standard star spectrum against rotationally broadened synthetic versions of itself (using PyAstronomy's *rotBroad* function; Gray 1976, 1992; White et al. 2007). To obtain our final  $v \sin i$  estimates, we average the  $v \sin i$  measurements for all orders, taking the standard deviation of these as the uncertainty, and then calculate the weighted average of resulting  $v \sin i$  estimates provided by 3 standard stars. We find that our measured radial and projected rotational velocities agree within 2 standard deviations of published literature values. Values are listed in Table 4.

### 3.3. Stellar Fundamental Parameters

We measure the stellar properties of the 38 observed stars using Empirical SpecMatch (Yee et al. 2017). This Python code determines stellar parameters of a spectrum by comparing it to a dense library of spectral stan-

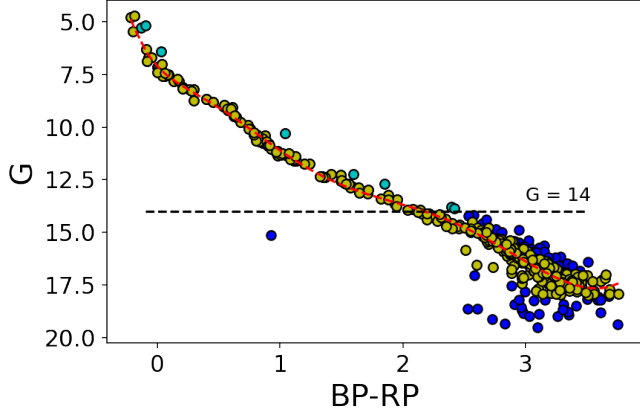


**Figure 5.** Candidate photometric binaries are identified in IC 2602 by an iterative fit to the main-sequence (down to  $G < 18$ ). Stars retained in the fit are shown as yellow circles. For stars brighter than  $G=14$ , any star more than 0.6 magnitudes above the fit are considered candidate binaries (cyan circles). For stars fainter than  $G=14$  (blue circles), we do not identify binaries because of the broader main sequence.

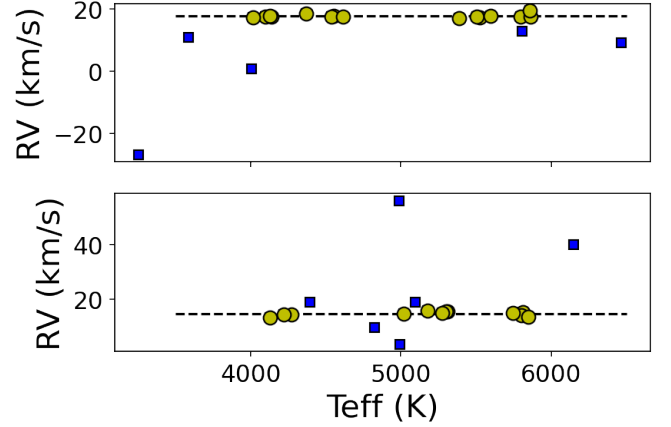


**Figure 6.** Distribution of RVs for spectroscopically observed stars in IC 2602 (*top panel*) and IC 2391 (*bottom panel*) as a function of effective temperature. Candidate binary stars (blue squares) are identified by iterative fits to the mean RVs (dotted black lines) of the ensembles; yellow circles are not candidate binaries.

dards. The code employs nonlinear least-squares minimization (Newville et al. 2014) to minimize  $\chi^2$  when (1) obtaining the best-matching library spectra, allowing continuum normalization and  $v \sin i$  provided by the SpecMatch program to float as free parameters, and (2) generating the best-matching linear combination of library spectra to determine stellar properties.

Figure 4 illustrates the best fit metallicities versus effective temperatures of candidate cluster members, along with the values of the comparison standards from which these values were determined. Stellar properties for the candidate double-lined spectroscopic binaries (including the two stars with  $[\text{Fe}/\text{H}] < -0.5$ ) marked in Tables 3 and 4 are unreliable due to contamination of spectra by companions.

Using previously known members to test Empirical SpecMatch, we find that our derived properties for single star members are consistent to within the uncertainties of published literature values (Marsden et al. 2009; De Silva et al. 2013; Randich et al. 2018). Best fit effective temperatures, surface gravities, and metallicities for new and know members are listed in Tables 3 and 4, respectively.

#### 4. NEW AND CANDIDATE BINARIES

We find new candidate photometric and spectroscopic binaries based on the following analyses.

##### 4.1. New Candidate Photometric Binaries

Unresolved multiple star systems with companions of comparable brightness are expected to be positioned above the single star main sequence (Cantat-Gaudin et

al. 2018). To identify candidate photometric binaries, we use 8th-order polynomials to iteratively fit the main sequences for stars brighter than  $G=18$  magnitude of these clusters. We classify candidate binary stars as those that sit above the fit by at least 0.6 magnitudes (see Figure 5); this is roughly 0.2 standard deviations above the best-fit main sequences. While we can be confident this prescription works down to  $G \sim 14$ , the prescription fails at dimmer magnitudes due to the spread in the main sequence. Considering only candidate members with  $G < 14$ , we identify 18 candidate photometric binaries. We find that 14 of these are previously known cluster members (7 in IC 2602 and 7 in IC 2391) while 4 are new (2 in IC 2602 and 2 in IC 2391). Candidate photometric binaries are marked in Tables 3 and 4.

##### 4.2. New Candidate Spectroscopic Binaries

Cluster members with RVs significantly different from the mean RVs of cluster stars may be spectroscopic binaries (Platais et al. 2007). To identify such candidate spectroscopic binaries, we iteratively fit the mean RVs of cluster stars within 3 standard deviations. To obtain the best fit (see Figure 6), we regard as candidate spectroscopic binaries those stars with RVs different from the resulting means of the ensembles by more than 3 km/s ( $\sim 1$  standard deviation). Given that the internal radial velocity dispersions of these clusters is expected to be less than 1 km/s (Stauffer et al. 1997), we have applied a more stringent constraint for our 43-52 Myr clusters than the prescription used by Hayes & Friel (2014) for 1-3 Gyr clusters (3 km/s vs. 5 km/s). The stars we do not flag as candidate spectroscopic binaries are used to

estimate the cluster’s radial velocities and dispersions in Section 6.

Of the 11 new candidate spectroscopic binaries we identify (5 in IC 2602, 6 in IC 2391), we find that 5 are double-lined (4 in IC 2602, 1 in IC 2391) and 6 are single-lined (1 in IC 2602, 5 in IC 2391). These binaries are marked in Tables 3 and 4.

## 5. CONFIRMATION OF NEW CANDIDATE MEMBERS

We use the presence of lithium absorption or H $\alpha$  emission to assign membership for candidate members. We observe that 19 of 20 IC 2602 stars show lithium absorption while 12 of 20 show H $\alpha$  emission; 11 stars show both. Furthermore, we observe that all 18 IC 2391 stars show lithium absorption while 5 of 18 show H $\alpha$  emission.

The double-lined spectroscopic binary, ALN 3, is the star without detectable lithium absorption noted above. While ALN 3 shows H $\alpha$  emission, a known youth indicator in pre-main-sequence stars (Barrado Y Navascués et al. 2000; Casey et al. 2016; Gutiérrez Albarrán et al. 2020), such emission can also be produced by close-interacting field binaries (Vesper & Honeycutt 1993; Wevers et al. 2016). Since it is still possible that ALN 3 has weak lithium absorption diluted by the flux of a companion, we regard the membership of ALN 3 to IC 2602 to be uncertain.

Based on consistent distances, sky positions, proper motions, and the presence of lithium absorption or H $\alpha$  emission, we conclude that 19 of 20 IC 2602 and 18 IC 2391 candidate members are bona-fide cluster members. In combination with previously known members, 133 (29%) of IC 2602 and 164 (47%) of IC 2391 are spectroscopically confirmed members. Measurements are listed and binarity is indicated for these stars in Tables 3 and 4.

## 6. ENSEMBLE CLUSTER PROPERTIES

We use the newly assembled measurements to determine ensemble cluster properties for IC 2602 and IC 2391. Using kinematic candidate members we identify in Section 2 (451 stars in IC 2602, 350 stars in IC 2391), we estimate new mean right ascensions, declinations, parallaxes, and proper motions for cluster stars. We compute mean distances using the values calculated by Bailer-Jones et al. (2018). For completeness, we list cluster ages from Bravi et al. (2018).

For spectroscopically determined properties, candidate spectroscopic binaries are excluded from the average cluster RVs and double-lined binaries are excluded from the average metallicities (see Section 4.2). In total,

**Table 2.** Summary of Ensemble Cluster Properties

Property	Value	Std. Dev.
<b>IC 2602</b>		
Center RA (deg)	160.524 $\pm$ 0.004	3.585(52 $\sigma_{mn}$ )
Center DEC (deg)	-64.387 $\pm$ 0.004	1.231(18 $\sigma_{mn}$ )
Avg. $\varpi$ (mas)	6.576 $\pm$ 0.004	0.170(2.2 $\sigma_{mn}$ )
Avg. $\mu_{\alpha} \cos \delta$ (mas/yr)	-17.740 $\pm$ 0.009	1.528(11 $\sigma_{mn}$ )
Avg. $\mu_{\delta}$ (mas/yr)	10.669 $\pm$ 0.008	1.530(12 $\sigma_{mn}$ )
Avg. Distance (pc)	151.58 $^{+1.87}_{-1.80}$	3.90(2.1 $\sigma_{mn}$ )
Age (Myr)	43.7 $^{+4.3}_{-3.9}$ (B18)	
Avg. RV (km/s)	17.73 $\pm$ 0.04	0.56(3.9 $\sigma_{mn}$ )
Avg. [Fe/H] (dex)	0.02 $\pm$ 0.02	0.07(0.8 $\sigma_{mn}$ )
<b>IC 2391</b>		
Center RA (deg)	130.276 $\pm$ 0.005	1.630(24 $\sigma_{mn}$ )
Center DEC (deg)	-52.923 $\pm$ 0.005	1.763(23 $\sigma_{mn}$ )
Avg. $\varpi$ (mas)	6.628 $\pm$ 0.005	0.228(2.9 $\sigma_{mn}$ )
Avg. $\mu_{\alpha} \cos \delta$ (mas/yr)	-25.005 $\pm$ 0.010	1.590(10 $\sigma_{mn}$ )
Avg. $\mu_{\delta}$ (mas/yr)	23.236 $\pm$ 0.011	1.609(10 $\sigma_{mn}$ )
Avg. Distance (pc)	150.44 $^{+1.86}_{-1.79}$	4.99(2.7 $\sigma_{mn}$ )
Age (Myr)	51.3 $^{+5.0}_{-4.5}$ (B18)	
Avg. RV (km/s)	14.88 $\pm$ 0.04	0.78(5.6 $\sigma_{mn}$ )
Avg. [Fe/H] (dex)	0.05 $\pm$ 0.02	0.07(0.8 $\sigma_{mn}$ )

*Notes.* Ensemble cluster property values and uncertainties are listed in Column 2 while standard deviations are compared with mean individual uncertainties ( $\sigma_{mn}$ ) in Column 3. Here, the reference B18 refers to Bravi et al. (2018).

15 IC 2602 and 12 IC 2391 stars are used to estimate mean RVs while 16 IC 2602 and 17 IC 2391 stars are used to estimate mean metallicities. Our measured ensemble values agree with literature values to within the uncertainties of previous estimates (as reported by Randich et al. 2001; Platais et al. 2007; Marsden et al. 2009).

IC 2602 has central positions at RA=160.524 $\pm$ 0.004 and DEC=-64.387 $\pm$ 0.004 degrees where errors represent uncertainties in the means. IC 2602 members have an average distance of 151.58 pc, with an uncertainty in the mean of  $\sim$ 1.8 pc and a standard deviation of 3.90 pc that is 2.1 times larger than the average distance uncertainty. IC 2602 members have a mean RV of 17.73 km/s with an uncertainty in the mean of 0.04 km/s and a standard deviation of 0.56 km/s that is 3.9 times larger than the average RV uncertainty.

IC 2391 has central positions at RA=130.276 $\pm$ 0.005 and DEC=-52.923 $\pm$ 0.005 degrees where errors represent uncertainties in the means. IC 2391 members have an average distance of 150.44 pc, with an uncertainty in the mean of  $\sim$ 1.8 pc and a standard deviation of 4.99 pc that



is 2.7 times larger than the average distance uncertainty. IC 2391 members have a mean RV of 14.88 km/s with an uncertainty in the mean of 0.04 km/s and a standard deviation of 0.78 km/s that is 5.6 times larger than the average RV uncertainty.

Given that the standard deviation of RVs is  $\sim 0.8$  km/s in IC 2391 and  $\sim 0.6$  km/s in IC 2602, we confirm that the standard deviations in these clusters is  $< 1$  km/s (Stauffer et al. 1997) and our results are in keeping with the claim that older clusters have larger RV dispersions (Hayes & Friel 2014). For the cluster properties we measure (with the exception of metallicity), standard deviations are larger than both ensemble and mean individual uncertainties. This implies that the observed spread in cluster properties is real and not an artifact of measurement errors. Values are assembled in Table 2.

## 7. SUMMARY

We use *Gaia* DR2 positions, space motions, and photometry to map out the stellar populations of IC 2602 and IC 2391. Using CHIRON spectra and Empirical SpecMatch, we determine stellar properties and measure signatures of youth for 38 stars. On the basis of this analysis, we obtain the following main results:

- We refine the single-star main sequences of IC 2602 (451 stars) and IC 2391 (350 stars). We find a large population of new candidate cluster members (331 stars in IC 2602, 198 stars in IC 2391), never reported before in the literature. The refined membership lists are useful for calibrating models of stellar evolution, planet formation and migration.

- We identify new candidate photometric (4 stars) and spectroscopic (10 stars) binaries; 6 of the latter are single-lined while 4 are double-lined. These findings can be used to improve binary fraction estimates in these clusters. If follow-up observations reveal them to be eclipsing binaries as well, the data can be used to improve stellar evolution models and relations.
- We determine radial and projected rotational velocities, equivalent widths of lithium and H $\alpha$ , effective temperatures, surface gravities, and metallicities for all 38 stars observed. We confirm that 13 IC 2602 and 12 IC 2391 new candidate members are bona-fide cluster members. This increases the known stellar populations of these clusters (120 stars in IC 2602; 152 stars in IC 2391) by 12% and 8% respectively.
- The data enable new, more precise ensemble stellar properties (Table 2).

## 8. ACKNOWLEDGMENTS

We are indebted to members of the SMARTS Consortium and NSF's National Optical-Infrared Astronomy Research Laboratory, especially the staff at CTIO, for efforts to keep the SMARTS/CTIO 1.5-m telescope and CHIRON spectrograph in operation. We give special thanks to Todd Henry, Wei-Chun Jao, Leonardo Paredes, Hodari-Sadiki James, Rodrigo Hinojosa, and Roberto Aviles for scheduling, observing, and reducing data for stars in the paper. This research has made use of the SIMBAD database, operated at CDS, Strasbourg, France. This research has made use of the VizieR catalogue access tool, CDS, Strasbourg, France (DOI : 10.26093/cds/vizie). The original description of the VizieR service was published in 2000, A&AS 143, 23.

**Table 3.** Measurements for 26 new candidate members of IC 2602 and IC 2391

Identifier		Measurements from CHIRON spectra				Stellar Parameters from SpecMatch		
Internal	2MASS	RV (km/s)	$v \sin i$ (km/s)	EW[Li] (Å)	EW[H $\alpha$ ] (Å)	Teff (K)	log(g) (dex)	[Fe/H] (dex)
<u>IC 2602</u>								
ALN 1	10420316-6520590	17.37 $\pm$ 0.12	7.6 $\pm$ 0.8	0.16 $\pm$ 0.01	0.76 $\pm$ 0.02	5527 $\pm$ 110	4.53 $\pm$ 0.12	-0.06 $\pm$ 0.09
ALN 2	10414173-6222205	17.06 $\pm$ 0.19	23.4 $\pm$ 2.2	0.35 $\pm$ 0.02	0.02 $\pm$ 0.01	5385 $\pm$ 110	4.50 $\pm$ 0.12	-0.03 $\pm$ 0.09
ALN 3 <sup>c</sup>	10411756-6526576	-26.69 $\pm$ 0.20	17.4 $\pm$ 5.6	<0.01 $\pm$ 0.01	-0.02 $\pm$ 0.01	3257 $\pm$ 70	4.86 $\pm$ 0.12	0.12 $\pm$ 0.09
ALN 4	10384893-6330430	17.69 $\pm$ 0.12	4.6 $\pm$ 1.8	0.05 $\pm$ 0.01	0.72 $\pm$ 0.03	4556 $\pm$ 110	4.60 $\pm$ 0.12	0.04 $\pm$ 0.09
ALN 5 <sup>a,c</sup>	10385502-6257272	10.88 $\pm$ 0.21	19.6 $\pm$ 6.4	0.02 $\pm$ 0.01	-0.24 $\pm$ 0.02	3586 $\pm$ 70	4.83 $\pm$ 0.12	-0.53 $\pm$ 0.09
ALN 6 <sup>c</sup>	10591218-6438089	9.28 $\pm$ 0.21	23.3 $\pm$ 6.6	0.02 $\pm$ 0.01	-0.11 $\pm$ 0.01	6465 $\pm$ 110	3.86 $\pm$ 0.12	0.18 $\pm$ 0.09
ALN 7	10322955-6506403	17.47 $\pm$ 0.17	13.6 $\pm$ 1.3	0.31 $\pm$ 0.02	-0.03 $\pm$ 0.01	4537 $\pm$ 110	4.61 $\pm$ 0.12	-0.01 $\pm$ 0.09
ALN 8	10482786-6554502	17.44 $\pm$ 0.16	9.2 $\pm$ 1.8	0.22 $\pm$ 0.03	-0.26 $\pm$ 0.02	4098 $\pm$ 70	4.68 $\pm$ 0.12	-0.04 $\pm$ 0.09
ALN 9	10200052-6217465	18.61 $\pm$ 0.15	7.7 $\pm$ 1.6	0.10 $\pm$ 0.01	-0.25 $\pm$ 0.02	4367 $\pm$ 70	4.65 $\pm$ 0.12	0.03 $\pm$ 0.09
ALN 10 <sup>b</sup>	10280304-6316132	0.68 $\pm$ 0.18	26.0 $\pm$ 4.2	0.09 $\pm$ 0.01	-0.63 $\pm$ 0.02	4006 $\pm$ 70	4.67 $\pm$ 0.12	0.19 $\pm$ 0.09
ALN 11	10521914-6558069	17.55 $\pm$ 0.15	7.4 $\pm$ 1.5	0.16 $\pm$ 0.02	-0.70 $\pm$ 0.02	4138 $\pm$ 70	4.66 $\pm$ 0.12	0.14 $\pm$ 0.09
ALN 12 <sup>a,c</sup>	10521708-6502488	12.78 $\pm$ 0.13	20.0 $\pm$ 5.6	0.10 $\pm$ 0.03	-1.30 $\pm$ 0.05	5804 $\pm$ 110	4.28 $\pm$ 0.12	-0.11 $\pm$ 0.09
ALN 13	10353048-6218367	17.40 $\pm$ 0.16	8.2 $\pm$ 1.8	0.20 $\pm$ 0.02	-0.85 $\pm$ 0.02	4017 $\pm$ 70	4.69 $\pm$ 0.12	0.04 $\pm$ 0.09
ALN 14	10315315-6234333	17.79 $\pm$ 0.17	13.0 $\pm$ 1.3	0.34 $\pm$ 0.02	-0.66 $\pm$ 0.02	4131 $\pm$ 70	4.67 $\pm$ 0.12	-0.01 $\pm$ 0.09
<u>IC 2391</u>								
NTC 1	08202510-5340306	15.95 $\pm$ 0.12	4.6 $\pm$ 2.0	0.22 $\pm$ 0.01	-0.22 $\pm$ 0.02	5175 $\pm$ 110	4.51 $\pm$ 0.12	0.09 $\pm$ 0.09
NTC 2	08320021-5539048	14.43 $\pm$ 0.16	9.5 $\pm$ 1.0	0.19 $\pm$ 0.02	-0.41 $\pm$ 0.02	4272 $\pm$ 70	4.66 $\pm$ 0.12	-0.02 $\pm$ 0.09
NTC 3 <sup>b</sup>	08365944-5219251	19.08 $\pm$ 0.14	7.0 $\pm$ 1.6	0.02 $\pm$ 0.01	0.55 $\pm$ 0.03	4395 $\pm$ 70	4.64 $\pm$ 0.12	0.04 $\pm$ 0.09
NTC 4	08372464-5254109	14.67 $\pm$ 0.16	7.9 $\pm$ 1.2	0.04 $\pm$ 0.01	-0.54 $\pm$ 0.02	4222 $\pm$ 70	4.66 $\pm$ 0.12	-0.02 $\pm$ 0.09
NTC 5	08383609-5206388	13.34 $\pm$ 0.21	27.2 $\pm$ 3.9	0.02 $\pm$ 0.01	-0.23 $\pm$ 0.01	4131 $\pm$ 70	4.67 $\pm$ 0.12	0.06 $\pm$ 0.09
NTC 6	08433845-5130289	15.76 $\pm$ 0.11	7.2 $\pm$ 0.7	0.15 $\pm$ 0.01	0.72 $\pm$ 0.02	5310 $\pm$ 110	4.48 $\pm$ 0.12	0.12 $\pm$ 0.09
NTC 7	08433893-5130249	15.73 $\pm$ 0.11	5.8 $\pm$ 2.3	0.20 $\pm$ 0.01	0.67 $\pm$ 0.02	5298 $\pm$ 110	4.47 $\pm$ 0.12	0.13 $\pm$ 0.09
NTC 8 <sup>b</sup>	08443450-5255325	18.88 $\pm$ 0.09	5.1 $\pm$ 1.4	0.02 $\pm$ 0.01	0.82 $\pm$ 0.02	5097 $\pm$ 110	4.54 $\pm$ 0.12	0.17 $\pm$ 0.09

**Table 3** *continued*

Table 3 (*continued*)

Identifier		Measurements from CHIRON spectra			Stellar Parameters from SpecMatch			
Internal	2MASS	RV (km/s)	$v \sin i$ (km/s)	EW[Li] (Å)	EW[H $\alpha$ ] (Å)	Teff (K)	log(g) (dex)	[Fe/H] (dex)
NTC 9 <sup>a,b</sup>	08473860-5216099	9.80±0.13	9.3±1.0	0.03±0.01	0.33±0.01	4823±110	4.46±0.12	0.00±0.09
NTC 10 <sup>b</sup>	08583097-5040359	3.77±0.11	7.0±1.0	0.04±0.01	0.76±0.02	4993±110	4.52±0.12	0.08±0.09
NTC 11 <sup>a</sup>	08583180-5040360	14.81±0.11	8.3±1.3	0.05±0.01	0.77±0.02	5018±110	4.55±0.12	-0.03±0.09
NTC 12 <sup>b</sup>	08593213-5106511	55.92±0.12	4.6±1.9	0.07±0.01	0.93±0.02	4987±110	4.53±0.12	0.01±0.09

*Notes.* New candidate binaries are indicated as <sup>a</sup>photometric, <sup>b</sup>single-lined spectroscopic, or <sup>c</sup>double-lined spectroscopic. Stars flagged as candidate double-lined spectroscopic binaries have diminished equivalent widths and SpecMatch properties so those measurements are suspect in the table.

Table 4. Measurements for 12 known members of IC 2602 and IC 2391

Name	Measurements from CHIRON spectra					Stellar Parameters from SpecMatch				
	RV (km/s)	RV Lit. (km/s)	$v \sin i$ (km/s)	$v \sin i$ Lit. (km/s)	EW[Li] (Å)	EW[Hα] (Å)	Teff (K)	Teff Lit. (K)	log(g) (dex)	[Fe/H] (dex)
<u>IC 2602</u>										
W79	17.53±0.11	17.4(R18)	7.8±1.0	8(M09)	0.13±0.01	0.83±0.02	5505±110	5500(M09)	4.52±0.12	-0.04±0.09
R1	17.90±0.11	18(M09)	8.4±0.9	<10(R01)	0.19±0.01	0.60±0.02	5596±110	5320(M09)	4.53±0.12	-0.09±0.09
R10	17.61±0.16	19(M09)	14.9±1.2	14(M09)	0.23±0.02	-0.08±0.01	4614±110	4520(M09)	4.60±0.12	0.05±0.09
R66	17.64±0.13	17.4(R18)	12.0±0.9	12(S97)	0.21±0.01	0.62±0.02	5795±110	5792(R18)	4.47±0.12	0.00±0.09
R70	17.43±0.11	17.4(R18)	10.8±1.1	11(S97)	0.13±0.01	0.88±0.01	5862±110	5854(R18)	4.51±0.12	0.09±0.09
SR3	19.40±0.13	15.3(Me09)	13.2±1.2	14.7(Me09)	0.20±0.01	0.89±0.01	5860±110	N/A	4.41±0.12	-0.06±0.09
<u>IC 2391</u>										
VXR16A	15.49±0.19	15.5(S97)	20.8±1.9	20.7(Me09)	0.36±0.02	-0.12±0.01	5810±110	5130(M09)	4.51±0.12	0.10±0.09
VXR22A	14.26±0.11	14.0(D13)	8.4±0.6	8(M09)	0.24±0.01	0.35±0.01	5800±110	5700(D13)	4.52±0.12	0.06±0.09
VXR70	13.83±0.16	13.8(D13)	15.9±0.8	16(M09)	0.20±0.01	0.59±0.02	5850±110	5819(R18)	4.42±0.12	-0.10±0.09
PMM4362	15.14±0.10	15.11(P107)	9.2±0.6	9.0(Me09)	0.20±0.01	0.91±0.01	5746±110	5740(M09)	4.52±0.12	0.05±0.09
SHJM6	15.20±0.13	15.2(D13)	10.9±0.8	10(M09)	0.23±0.01	0.33±0.01	5276±110	5210(M09)	4.48±0.12	0.15±0.09
L37 <sup>a,c</sup>	39.81±0.13	31.69(Me09)	11.0±1.4	11.8(Me09)	0.07±0.00	0.64±0.01	6150±110	5900(M09)	4.09±0.12	-0.54±0.09

*Notes.* Known binaries are indicated as <sup>a</sup>photometric, <sup>b</sup>single-lined spectroscopic, or <sup>c</sup>double-lined spectroscopic. Stars flagged as known double-lined spectroscopic binaries have diminished equivalent widths and SpecMatch properties so those measurements are suspect in the table. The references are as follows: D13 = De Silva et al. 2013, M09 = Marsden et al. 2009 Me09 = Mermilliod et al. 2009, P107 = Platais et al. 2007, R01 = Randich et al. 2001, R18 = Randich et al. 2018, S97 = Stauffer et al. 1997.

## APPENDIX



Table A.1. Refined Membership List of IC 2391

2MASS	RA (h:m:s)	DEC (d:m:s)	$\varpi$ (mas)	$\epsilon_{\varpi}$ (mas)	$\mu_{\alpha} \cos \delta$ (mas/yr)	$\epsilon_{\mu_{\alpha} \cos \delta}$ (mas/yr)	$\mu_{\delta}$ (mas)	$\epsilon_{\mu_{\delta}}$ (mas/yr)	G (mag)	BP-RP (mag)
08422538-5306501	08:42:25.34	-53:06:49.97	7.11	0.23	-24.58	0.38	22.77	0.46	4.78	-0.24
08392384-5326230	08:39:23.80	-53:26:22.80	6.53	0.14	-25.79	0.31	21.19	0.32	5.42	-0.21
08395759-5303170	08:39:57.55	-53:03:16.65	6.76	0.21	-25.43	0.39	22.32	0.40	5.14	-0.20
08401759-5255190	08:40:17.54	-52:55:18.54	6.59	0.41	-30.56	0.78	21.43	0.76	3.47	-0.19
08401745-5300554	08:40:17.42	-53:00:55.07	6.46	0.09	-24.79	0.17	23.08	0.16	5.52	-0.18

*Notes.* Example data for IC 2391 candidate cluster members identified using the prescription in Section 2. The complete table of 350 candidate members is provided online. Here, the astrometric and photometric parameter values are concatenated to two decimal places.

Table A.2. Refined Membership List of IC 2602

2MASS	RA (h:m:s)	DEC (d:m:s)	$\varpi$ (mas)	$\epsilon_{\varpi}$ (mas)	$\mu_{\alpha} \cos \delta$ (mas/yr)	$\epsilon_{\mu_{\alpha} \cos \delta}$ (mas/yr)	$\mu_{\delta}$ (mas)	$\epsilon_{\mu_{\delta}}$ (mas/yr)	G (mag)	BP-RP (mag)
10465124-6423005	10:46:51.18	-64:23:00.35	6.34	32.8	-18.92	0.33	9.45	0.30	4.78	-0.22
10401142-6506006	10:40:11.40	-65:06:00.59	6.49	56.38	-19.31	0.20	9.56	0.19	5.45	-0.20
10440694-6357400	10:44:06.87	-63:57:39.71	6.81	14.69	-15.03	0.45	11.41	0.56	4.72	-0.19
10461656-6430526	10:46:16.51	-64:30:52.25	6.41	60.2	-16.19	0.20	10.85	0.18	5.28	-0.13
10462961-6415475	10:46:29.55	-64:15:47.51	6.76	38.7	-17.9	0.29	9.54	0.27	5.17	-0.10

*Notes.* Example data for IC 2602 candidate cluster members identified using the prescription in Section 2. The complete table of 451 candidate members is provided online. Here, the astrometric and photometric parameter values are concatenated to two decimal places.

## REFERENCES

- Abt, H. A. & Morgan, W. W. 1972, *ApJL*, 174, L131.  
doi:10.1086/180965
- Bailer-Jones, C. A. L., Rybizki, J., Fouesneau, M., et al. 2018, *AJ*, 156, 58. doi:10.3847/1538-3881/aacb21
- Baraffe, I., Homeier, D., Allard, F., et al. 2015, *A&A*, 577, A42. doi:10.1051/0004-6361/201425481
- Barrado y Navascués, D., Stauffer, J. R., & Patten, B. M. 2000, *Stellar Clusters and Associations: Convection, Rotation, and Dynamos*, 198, 269
- Barrado y Navascués, D., Stauffer, J. R., Briceño, C., et al. 2001, *ApJS*, 134, 103. doi:10.1086/320359
- Barrado y Navascués, D., Stauffer, J. R., & Jayawardhana, R. 2004, *ApJ*, 614, 386. doi:10.1086/423485
- Boudreault, S. & Bailer-Jones, C. A. L. 2009, *ApJ*, 706, 1484. doi:10.1088/0004-637X/706/2/1484
- Braes, L. L. E. 1962, *BAN*, 16, 297
- Brandt, T. D. & Huang, C. X. 2015, *ApJ*, 807, 24. doi:10.1088/0004-637X/807/1/24
- Bravi, L., Zari, E., Sacco, G. G., et al. 2018, *A&A*, 615, A37. doi:10.1051/0004-6361/201832645
- Briceno, C., Calvet, N., Hernandez, J., et al. 2018, arXiv:1805.01008
- Buscombe, W. 1965, *MNRAS*, 129, 411. doi:10.1093/mnras/129.6.411
- Butler, R. P., Marcy, G. W., Williams, E., et al. 1996, *PASP*, 108, 500. doi:10.1086/133755
- Cantat-Gaudin, T., Jordi, C., Vallenari, A., et al. 2018, *A&A*, 618, A93. doi:10.1051/0004-6361/201833476
- Casey, A. R., Ruchti, G., Masseron, T., et al. 2016, *MNRAS*, 461, 3336. doi:10.1093/mnras/stw1512
- Cayrel, R. 1988, *The Impact of Very High S/N Spectroscopy on Stellar Physics*, 132, 345
- Cummings, J. D., Deliyannis, C. P., Maderak, R. M., et al. 2017, *AJ*, 153, 128. doi:10.3847/1538-3881/aa5b86
- D’Orazi, V. & Randich, S. 2009, *A&A*, 501, 553. doi:10.1051/0004-6361/200811587
- D’Orazi, V., De Silva, G. M., & Melo, C. F. H. 2017, *A&A*, 598, A86. doi:10.1051/0004-6361/201629888
- De Silva, G. M., D’Orazi, V., Melo, C., et al. 2013, *MNRAS*, 431, 1005. doi:10.1093/mnras/stt153
- Deliyannis, C. P., Pinsonneault, M. H., & Duncan, D. K. 1993, *ApJ*, 414, 740. doi:10.1086/173120
- Deliyannis, C. P., Anthony-Twarog, B. J., Lee-Brown, D. B., et al. 2019, *AJ*, 158, 163. doi:10.3847/1538-3881/ab3fad
- Dobbie, P. D., Lodieu, N., & Sharp, R. G. 2010, *MNRAS*, 409, 1002. doi:10.1111/j.1365-2966.2010.17355.x
- Dodd, R. J. 2004, *MNRAS*, 355, 959. doi:10.1111/j.1365-2966.2004.08378.x
- Drimmel, R., Bucciarelli, B., & Inno, L. 2019, *Research Notes of the American Astronomical Society*, 3, 79. doi:10.3847/2515-5172/ab2632
- Eastman, J., Gaudi, B. S., & Agol, E. 2013, *PASP*, 125, 83. doi:10.1086/669497
- Eggen, O. J. 1975, *PASP*, 87, 37. doi:10.1086/129722
- Eggen, O. J. 1983a**, *MNRAS*, 204, 377. doi:10.1093/mnras/204.2.377
- Eggen, O. J. 1983b**, *MNRAS*, 204, 391. doi:10.1093/mnras/204.2.391
- Eggen, O. J. 1991, *AJ*, 102, 2028. doi:10.1086/116025
- Esplin, T. L. & Luhman, K. L. 2019, *AJ*, 158, 54. doi:10.3847/1538-3881/ab2594
- Feinstein, A. 1961, *PASP*, 73, 410. doi:10.1086/127722
- Foster, D. C., Byrne, P. B., Hawley, S. L., et al. 1997, *A&AS*, 126, 81. doi:10.1051/aas:1997251
- Gagné, J., Mamajek, E. E., Malo, L., et al. 2018, *ApJ*, 856, 23. doi:10.3847/1538-4357/aaae09
- Gaia Collaboration, Babusiaux, C., van Leeuwen, F., et al. 2018, *A&A*, 616, A10. doi:10.1051/0004-6361/201832843
- Gaidos, E., Mann, A. W., Rizzuto, A., et al. 2017, *MNRAS*, 464, 850. doi:10.1093/mnras/stw2345
- Gray, D. F. 1976, *A Wiley-Science Publication*, New York: Wiley, 1976
- Gray, D. F. 1992, *Camb. Astrophys. Ser.*, Vol. 20,
- Gutiérrez Albarrán, M. L., Montes, D., Gómez Garrido, M., et al. 2020, *A&A*, 643, A71. doi:10.1051/0004-6361/202037620
- Hayes, C. R. & Friel, E. D. 2014, *AJ*, 147, 69. doi:10.1088/0004-6256/147/4/69
- Jones, J., White, R. J., Boyajian, T., et al. 2015, *ApJ*, 813, 58. doi:10.1088/0004-637X/813/1/58
- Lada, C. J. & Lada, E. A. 2003, *ARA&A*, 41, 57. doi:10.1146/annurev.astro.41.011802.094844
- Levato, H., Garcia, B., Lousto, C., et al. 1988, *Ap&SS*, 146, 361. doi:10.1007/BF00637586
- Lindgren, L., Hernández, J., Bombrun, A., et al. 2018, *A&A*, 616, A2. doi:10.1051/0004-6361/201832727
- Lodieu, N., Pérez-Garrido, A., Smart, R. L., et al. 2019, *A&A*, 628, A66. doi:10.1051/0004-6361/201935533
- Luhman, K. L. & Esplin, T. L. 2020, *AJ*, 160, 44. doi:10.3847/1538-3881/ab9599
- Lyngå, G. 1962, *Arkiv for Astronomi*, 3, 65
- Mann, A. W., Gaidos, E., Vanderburg, A., et al. 2017, *AJ*, 153, 64. doi:10.1088/1361-6528/aa5276
- Marsden, S. C., Carter, B. D., & Donati, J.-F. 2009, *MNRAS*, 399, 888. doi:10.1111/j.1365-2966.2009.15319.x
- Merle, T., Van Eck, S., Jorissen, A., et al. 2017, *A&A*, 608, A95. doi:10.1051/0004-6361/201730442

- 578 Mermilliod, J.-C., Mayor, M., & Udry, S. 2009, *A&A*, 498,  
579 949. doi:10.1051/0004-6361/200810244
- 580 Messina, S., Pizzolato, N., Guinan, E. F., et al. 2003, *A&A*,  
581 410, 671. doi:10.1051/0004-6361:20031203
- 582 Newville, M., Stensitzki, T., Allen, D. B., et al. 2014,  
583 Zenodo
- 584 Ochsenbein, F., Bauer, P., & Marcout, J. 2000, *A&AS*, 143,  
585 23. doi:10.1051/aas:2000169
- 586 Paulson, D. B. & Yelda, S. 2006, *PASP*, 118, 706.  
587 doi:10.1086/504115
- 588 Pecaut, M. J. & Mamajek, E. E. 2013, *ApJS*, 208, 9.  
589 doi:10.1088/0067-0049/208/1/9
- 590 Platais, I., Melo, C., Mermilliod, J.-C., et al. 2007, *A&A*,  
591 461, 509. doi:10.1051/0004-6361:20065756
- 592 Quinn, S. N. & White, R. J. 2016, *ApJ*, 833, 173.  
593 doi:10.3847/1538-4357/833/2/173
- 594 Ragusa, E., Rosotti, G., Teyssandier, J., et al. 2018,  
595 *MNRAS*, 474, 4460. doi:10.1093/mnras/stx3094
- 596 Randich, S., Aharpour, N., Pallavicini, R., et al. 1997,  
597 *A&A*, 323, 86
- 598 Randich, S., Pallavicini, R., Meola, G., et al. 2001, *A&A*,  
599 372, 862. doi:10.1051/0004-6361:20010339
- 600 Randich, S., Primas, F., Pasquini, L., et al. 2002, *A&A*,  
601 387, 222. doi:10.1051/0004-6361:20020355
- 602 Randich, S., Bragaglia, A., Pastori, L., et al. 2005, *The*  
603 *Messenger*, 121, 18
- 604 Randich, S., Tognelli, E., Jackson, R., et al. 2018, *A&A*,  
605 612, A99. doi:10.1051/0004-6361/201731738
- 606 Richer, H. B., Caiazzo, I., Du, H., et al. 2021, *ApJ*, 912,  
607 165. doi:10.3847/1538-4357/abdeb7
- 608 Rolleston, W. R. J. & Byrne, P. B. 1997, *A&AS*, 126, 357.  
609 doi:10.1051/aas:1997270
- 610 Simon, T. & Patten, B. M. 1998, *PASP*, 110, 283.  
611 doi:10.1086/316131
- 612 Spina, L., Randich, S., Magrini, L., et al. 2017, *A&A*, 601,  
613 A70. doi:10.1051/0004-6361/201630078
- 614 Stauffer, J. R., Hartmann, L. W., Prosser, C. F., et al.  
615 1997, *ApJ*, 479, 776. doi:10.1086/303930
- 616 Tokovinin, A., Fischer, D. A., Bonati, M., et al. 2013,  
617 *PASP*, 125, 1336. doi:10.1086/674012
- 618 Torres, C. A. O., Quast, G. R., Melo, C. H. F., et al. 2008,  
619 *Handbook of Star Forming Regions*, Volume II, 757
- 620 Vesper, D. N. & Honeycutt, R. K. 1993, *PASP*, 105, 731.  
621 doi:10.1086/133224
- 622 Wenger, M., Ochsenbein, F., Egret, D., et al. 2000, *A&AS*,  
623 143, 9. doi:10.1051/aas:2000332
- 624 Wevers, T., Hodgkin, S. T., Jonker, P. G., et al. 2016,  
625 *MNRAS*, 458, 4530. doi:10.1093/mnras/stw643
- 626 White, R. J., Gabor, J. M., & Hillenbrand, L. A. 2007, *AJ*,  
627 133, 2524. doi:10.1086/514336
- 628 Whiteoak, J. B. 1961, *MNRAS*, 123, 245.  
629 doi:10.1093/mnras/123.3.245
- 630 Wright, J. T. & Eastman, J. D. 2014, *PASP*, 126, 838.  
631 doi:10.1086/678541
- 632 Wu, Z.-Y., Zhou, X., Ma, J., et al. 2009, *MNRAS*, 399,  
633 2146. doi:10.1111/j.1365-2966.2009.15416.x
- 634 Yee, S. W., Petigura, E. A., & von Braun, K. 2017, *ApJ*,  
635 836, 77. doi:10.3847/1538-4357/836/1/77
- 636 Zuckerman, B., Klein, B., & Kastner, J. 2019, *ApJ*, 887, 87.  
637 doi:10.3847/1538-4357/ab45ea